

Entanglement Amplification in the Non-Perturbative Dynamics of Modular Quantum Systems

A. Bayat¹, S. M. Giampaolo², F. Illuminati², and M. B. Plenio¹

¹*Institut für Theoretische Physik, Albert-Einstein-Allee 11, Universität Ulm, D-89069 Ulm, Germany*

²*Dipartimento di Ingegneria Industriale, Università degli Studi di Salerno, Via Ponte don Melillo, I-84084 Fisciano (SA), Italy*

(Dated: March 12, 2013)

We analyze the conditions for entanglement amplification between distant and not directly interacting quantum objects by their common coupling to media with static modular structure and subject to a local (single-bond) quenched dynamics. We show that in the non-perturbative regime of the dynamics the initial end-to-end entanglement is strongly amplified and, moreover, can be distributed efficiently between distant objects. Due to its intrinsic local and non-perturbative nature the dynamics is fast and robust against thermal fluctuations, and its control is undemanding. We show that the origin of entanglement amplification lies in the interference of the ground state and at most one of the low-lying energy eigenstates. The scheme can be generalized to provide a fast and efficient router for generating entanglement between simultaneous multiple users.

PACS numbers: 03.67.-a, 03.67.Hk, 03.65.Ud, 75.10.Pq, 75.20.Hr

I. INTRODUCTION

Realizing a sizable and stable entanglement between distant qubits is a crucial stage in performing quantum information and communication tasks [1]. In the ground state of noncritical strongly correlated systems with short-range interactions the 2-points correlation functions and thus the entanglement between spins vanish exponentially with the distance [2]. To overcome this problem, a possibility is to mediate indirect interactions between distant qubits by a suitable quantum many-body medium. For instance, one can exploit impurities weakly coupled to the ends of a spin chain to create a strong long-distance entanglement between them [3]. Indeed a relatively large family of many-body systems allows for this possibility [4–6]. However, for most of these systems the energy gap is exponentially decreasing in the size of the system, so that even for short chains the mechanism becomes thermally unstable: very small thermal fluctuations are sufficient to mix the ground state with higher energy eigenstates and suppress the entanglement between the end impurities. One can introduce systems with interaction patterns such that the gap closes algebraically with the distance [4] at the price of letting the end-to-end entanglement become weakly decreasing with the size of the system [4, 5]. Even if all these results can be extended to higher dimensional systems [7] this appears to be the unavoidable limit of a purely static, ground-state approach [8]

On the other hand, it is well known that properly tailored time evolutions can propagate entanglement through many-body systems [9]. In particular, global [10] or local quantum quenches [11–15] can create long-distance entanglement. Apart from certain perturbative proposals that suffer from a very slow convergence [11–14], the dynamical schemes in general do not require the weak end coupling assumption [9, 10, 15, 16] and hence they hold a greater resistance against thermal instability but at the price of a much more elaborate control on the system. In conclusion, entangling distant qubits can be realized either via static or dynamic approaches, however, either at the price of a strong thermal instability or an excessively demanding control.

In the present work we introduce a scheme that combines the modular-static and the quench-dynamic approaches to en-

tanglement generation and distribution among distant qubits. The proposed mixed scheme strongly reduces the drawbacks of both approaches and realizes a novel mechanism of entanglement amplification starting from weakly entangled inputs. In our model, a quantum spin chain is split into two elementary bulk modules. Two end impurities are attached to each module with couplings of arbitrary strength. This initial static configuration is then evolved through a sudden quench of the bond connecting the two modules. We show that the generated end-to-end entanglement across the entire system is always larger than the initial entanglement at the ends of each module and that this *entanglement amplification* can always be achieved for all parameter ranges. As the length of each module is half the total size of the system and the impurity couplings are non perturbative, the energy gap remains sizable and thus thermal stability is assured. Moreover, by exploiting just a single bond quench for inducing a nontrivial dynamics, the required control is minimal. This mechanism can demonstrate an entanglement router which unlike previous proposals neither needs AC-control of the couplings [17] nor the presence of both ferromagnetic and anti-ferromagnetic couplings simultaneously [18]. Furthermore, the entanglement amplification mechanism finds a clear physical explanation in the quantum interference between only two eigenvectors of the final Hamiltonian.

II. INTRODUCING THE MODEL

We consider two chains of qubits, the *modules*, each constituted by a bulk of spins coupled at both ends with two impurities. The Hamiltonian of each module reads:

$$H_k = J'_k J(h_{1,2}^{(k)} + h_{N_k-1,N_k}^{(k)}) + J \sum_{i=2}^{N_k-2} h_{i,i+1}^{(k)},$$

$$h_{i,j}^{(k)} = X_i^{(k)} X_j^{(k)} + Y_i^{(k)} Y_j^{(k)} + \delta Z_i^{(k)} Z_j^{(k)}, \quad (1)$$

where $k = L, R$ denotes the left or right module, respectively with $N_k = N_L, N_R$ spins, $\{X_i^{(k)}, Y_i^{(k)}, Z_i^{(k)}\}$ are the Pauli spin operators at site i in the k -th module, $J > 0$ is the

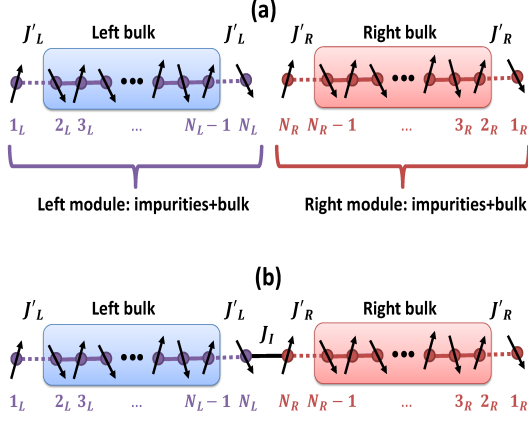


FIG. 1: (Color online) (a) A schematic picture of two independent modules and their couplings to the respective end impurities. (b) Onset of a quenched interaction dynamics between the two modules by switching on instantaneously a strong bond J_I between the impurities at the module-module boundary.

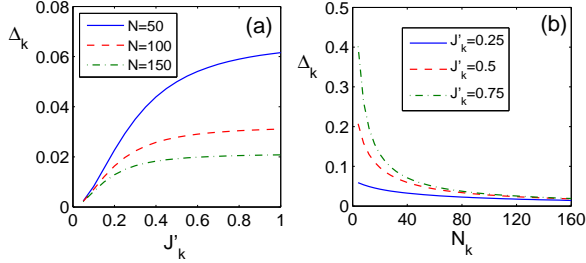


FIG. 2: (Color online) Energy gap Δ_k of a single XX module as a function of: (a) the coupling J'_k to the end impurities for different sizes N_k of the module; (b) the size N_k for different values of J'_k .

exchange spin-spin coupling strength, the dimensionless parameter $J'_k > 0$ specifies the coupling to the end impurities, and δ is the interaction anisotropy along the z direction. A schematic picture of this system is shown in Fig. 1 (a) (note the mirror inversion of spin numbering in each module). The spin-1/2 XXZ Hamiltonian Eq. (1) for each module has a rich zero-temperature quantum phase diagram; in particular, for $-1 \leq \delta \leq 1$, the system is in the so-called gapless XY antiferromagnetic phase that admits a nondegenerate, highly entangled ground state. In the two fully isotropic limits one recovers the relevant cases of the XX Hamiltonian ($\delta=0$) and the Heisenberg (XXX) Hamiltonian ($\delta=1$).

III. STATIC END-TO-END ENTANGLEMENT IN MODULES

The model in Eq. (1) exhibits long-distance entanglement in the ground state when the module has *even* length N_k and $J'_k < J$ so that the spins in the bulk tend to entangle between themselves and consequently the two end impurities are

forced to get entangled [4, 5]. From the ground state of the XXZ Hamiltonian H_k , one can compute the initial reduced density matrix of the two impurities by tracing out the spins of the bulk. Due to the symmetries of the system, the reduced state is diagonal in the Bell basis

$$\rho_{1_k, N_k} = P_k^s |\psi^-\rangle \langle \psi^-| + \sum_{\alpha=x,y,z} P_k^\alpha |B^\alpha\rangle \langle B^\alpha|, \quad (2)$$

where $|\psi^-\rangle$ is the singlet state, P_k^s is the singlet fraction, $|B^\alpha\rangle$ (for $\alpha = x, y, z$) are the other Bell states which can be obtained by applying the α Pauli operator on one part of the singlet, and the P_k^α 's account for their contributions. For a fixed length N_k , one can increase P_k^s arbitrarily and create large entanglement between the two impurities by decreasing J'_k . However, by decreasing J'_k the energy gap of the system also decreases, at best algebraically [4, 5]; when the thermal energy $k_B T$ becomes comparable with the gap, the state of the system becomes a mixed thermal state with no entanglement between the end impurities. In Fig. 2(a) the energy gap Δ_k is plotted as a function of J'_k for a XX module of length N_k which clearly shows an exponential decay for small J'_k 's. Of course, the gap also decays with the size N_k as shown in Fig. 2(b).

IV. DYNAMICAL ENTANGLEMENT GENERATION IN A MODULAR QUANTUM SPIN CHAIN

Given the initial static situation with the two modules in their respective ground states, we introduce a quench dynamics between them. The two even-sized modules of lengths N_L and N_R are described via the Hamiltonians H_L and H_R introduced in Eq. (1). The exchange coupling J and anisotropic parameter δ are assumed to be identical in both modules, while the couplings with the end impurities are respectively J'_L and J'_R . The initial ground state of a chain of total length $N = N_L + N_R$ formed by the two noninteracting modules is obviously the tensor product of the ground states of the two subsystems: $|\psi(0)\rangle = |GS_L\rangle \otimes |GS_R\rangle$. At $t=0$ one switches on the interaction between the two modules:

$$H_I = J_I J (X_{N_L}^{(L)} X_{N_R}^{(R)} + Y_{N_L}^{(L)} Y_{N_R}^{(R)} + \delta Z_{N_L}^{(L)} Z_{N_R}^{(R)}), \quad (3)$$

where the dimensionless parameter J_I is the bond that couples the two modules. The total Hamiltonian of the system at $t > 0$ becomes, as schematically represented in Fig. 1(b), $H_T = H_L + H_R + H_I$. The initial product state is not an eigenvector of H_T and the system evolves according to $|\psi(t)\rangle = e^{-iH_T t} |\psi(0)\rangle$. The reduced state of the two end impurities at time t is

$$\rho_{1_L, 1_R}(t) = P_{out}^s(t) |\psi^-\rangle \langle \psi^-| + \sum_{\alpha=x,y,z} P_{out}^\alpha(t) |B^\alpha\rangle \langle B^\alpha|.$$

We use relative entropy of entanglement [19] as an operational measure to quantify the entanglement content of the two end-impurities at sites 1_L and 1_R defined by

$$E_{1_L, 1_R}(t) = 1 - H(P_{out}^s(t)) \quad (4)$$

where $H(x) = -x \log_2 x - (1-x) \log_2 (1-x)$. This is of course related to the concurrence [20] of the two impurities $C_{1_L, 1_R}(t)$ via $E_{1_L, 1_R}(t) = 1 - H((C_{1_L, 1_R}(t) + 1)/2)$ and always give a lower value with respect to concurrence.

A. Perturbative regime

We first study the case of J'_L and J'_R both sufficiently small so that the pairs of end impurities in each module are initially highly entangled (strong initial end-to-end entanglement in both modules). In this situation, in each module the impurities are effectively decoupled from the rest of the system and resorting to the Schrieffer-Wolff transformation [21] one obtains an effective interaction Hamiltonian for the impurities in each module

$$H_{eff}^k = J_{eff}^k (X_{1_k}^k X_{N_k}^k + Y_{1_k}^k Y_{N_k}^k + \delta Z_{1_k}^k Z_{N_k}^k), \quad (5)$$

where the effective coupling is linear in the energy gap: $J_{eff}^k = \Delta_k/4$ with $k = L, R$. Fixing the inter-module interaction bond at $J_I = J_{eff}^L + J_{eff}^R$, as shown in Fig. 1(b), one has that $E_{1_L, 1_R}(t) = 1 - H\left(\frac{5 - 3 \cos(4J_I t)}{8}\right)$. Therefore, at the optimal time $t_{opt} = \frac{\pi}{4J_I}$, the maximal long-distance entanglement is established between the ending sites. Compared to the static case with a single long module of length N with the same entanglement between the end impurities 1_L and 1_R , the dynamical mechanism in the perturbative regime assures a larger thermal stability "per se". If the entangling time t_{opt} is engineered so to be much smaller than the thermalization time, then the thermal effects are fully determined by the thermal initial state associated to the energy gap of each module, which is always above and can be made much larger than the gap of the two combined in a single one of size $N = N_L + N_R$. In the dynamic case one can exploit larger impurity couplings J'_k for each module in comparison to the static case with a single module of size N , thus increasing the gap, as illustrated in Fig. 2(a). In this way thermal instability is ameliorated but not fixed; moreover, the perturbative nature of the coupling J_I implies a very slow dynamics.

B. Non-perturbative regime: Entanglement amplification

When the strength of the coupling to the impurities becomes comparable to the interaction energies in the bulk, the initial end-to-end entanglement for each module is strongly suppressed, the reduction to the effective Hamiltonians Eq. (5) is no longer justified, and J_I cannot be determined analytically as in the perturbative regime. To proceed, one can observe that in practice the affordable time for the entangling dynamics is ultimately bounded by the decoherence rates. Introducing such upper bounds for the optimal entangling time, we define an optimization problem for the largest attainable end-to-end entanglement that depends on two free parameters, i.e. the static coupling to the end impurities $J' = J'_L = J'_R$ and the quench-dynamic bond J_I between the two modules. In Fig. 3(a) the end-to-end entanglement $E_{1_L, 1_R}(t)$ is plotted as

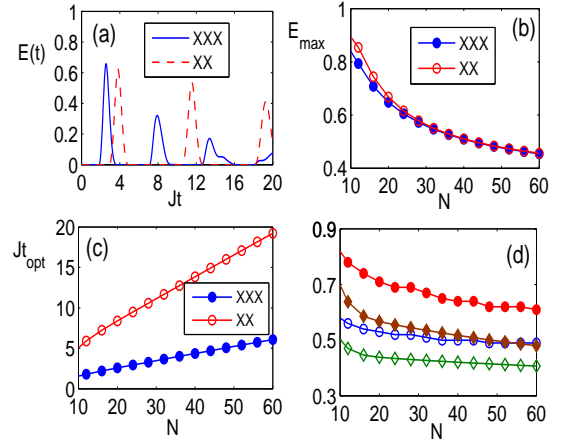


FIG. 3: (Color online) (a) End-to-end entanglement as a function of time for $N_L = N_R = 10$, $J' = 0.5$ and $J_I = 0.65$. (b) E_{max} as a function of N . (c) Optimal time t_{opt} versus length N . (d) Optimal impurity coupling J'_{opt} for XXX (open blue circles) and XX (green open diamonds) and optimal interaction coupling J_I^{opt} for XXX (filled red circles) and XX (filled brown diamonds).

a function of time both for the Heisenberg and the XX Hamiltonians. As reported in Fig. 3(a), in both the two cases for such a choice of J' and J_I , the time evolution after the quench generates a large end-to-end entanglement, strongly amplified respect to the initial one in each module. The optimal entangling time t_{opt} is then the earliest time at which the end-to-end entanglement peaks, defining its maximum attainable value: $E_{max} = E(t_{opt})$. In Fig. 3(b) we plot E_{max} as a function of the total chain's size N when both J' and J_I are tuned to their optimal values. One has that for long enough chains both the XX and Heisenberg Hamiltonians perform equally well. However, if we look at Fig. 3(c), where t_{opt} is reported as a function of N , one can see that the Heisenberg chain generates a faster dynamics with earlier peaks, an important added value in order to minimize the effects of decoherence. Finally, in Fig. 3(d) we report the optimal values J'_{opt} and J_I^{opt} , respectively of the coupling to the end impurities and the interaction coupling in the bulk, as functions of N . Remarkably, as Fig. 3(d) clearly shows, one finds that the optimal couplings decrease very slowly by increasing the size N , implying the onset of a fast dynamics and the permanence of the non-perturbative regime even for very long chains. Furthermore, larger couplings in Heisenberg chains in compare to XX ones results in a faster dynamics and provides higher energy gap and thus higher thermal stability.

To show how entanglement is actually amplified by the dynamical process we compare the initial static end-to-end entanglement $E_{1_L, N_L}(0)$ in the ground state of a single module of length $N_L = N/2$ and the output dynamical end-to-end entanglement $E_{1_L, 1_R}(t_{opt})$ at the optimal entangling time across two interacting modules forming a chain of total length $N_L + N_R = N$. Fig. 4(a) shows that the initial ground-state end-to-end entanglement is *always* amplified for the entire range of couplings J' to the end impurities. A remarkable rebound of $E_{1_L, 1_R}(t_{opt})$ occurs at a point of non-analyticity that sep-

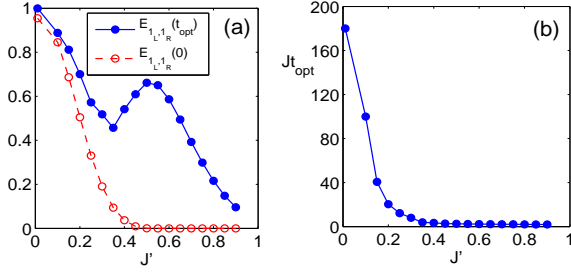


FIG. 4: (Color online) (a) The initial, static end-to-end entanglement $E_{1_L, N_L}(0)$ (or $E_{1_R, N_R}(0)$) in each single module of length $N_L = N_R = 10$ together with the maximal end-to-end dynamical entanglement $E_{1_L, 1_R}(t_{opt})$ for the entire two-module chain of length $N = N_L + N_R$ as functions of the dimensionless coupling J' for $\delta = 1$. (b) The optimal time Jt_{opt} (in the units of \hbar) at which entanglement peaks, as a function of J' .

arates the perturbative from the non-perturbative regime, corresponding to the onset of enhanced dynamical amplification against pure decay. In order to characterize and understand these two different regimes and the transition between them we have studied the entangling time t_{opt} as a function of the coupling J' to the end impurities. Fig. 4 (b) illustrates that in the perturbative regime t_{opt} increases exponentially with decreasing J' , while in the non-perturbative regime it remains essentially flat at very small values, guaranteeing, for appropriately chosen values of J' , that maximal amplification occurs well in advance of the effects of decoherence.

V. ORIGIN OF AMPLIFICATION: EXCITATION SPECTRUM AND QUANTUM INTERFERENCE

To understand the physical mechanism underlying entanglement amplification in the non-perturbative dynamics of modular many-body systems we must take notice of the fact that $|\psi(t)\rangle = \sum_{n=1}^{2^N} c_n e^{-iE_n t} |E_n\rangle$, where, $E_n(|E_n\rangle)$ is the n -th eigenvalue (eigenvector) of H_T and $c_n = \langle E_n | \psi(0) \rangle$. When the values of the Hamiltonian parameters J' and J_I are far from their optimal values, many of c_n 's are significantly different from zero. At values close to the optimal set the situation becomes radically different, as reported in Figs. 5(a) and (b), where the squared amplitudes $|c_n|^2$ are plotted as functions of the energy difference between the corresponding n -th eigenstate and the ground state of H_T , respectively for the XX ($\delta = 0$, Fig. 5(a)) and the Heisenberg Hamiltonian ($\delta = 1$, Fig. 5(b)). In both cases the initial state is essentially projected onto only two eigenstates of H_T , the ground state and just one of the first few low-lying excited states. Therefore the evolution of the initial state at time t under the action of H_T is essentially due to the relative phase factor $\phi(t) = \exp(-i\omega_\delta t)$, where ω_δ is the difference of the eigenvalues of the two eigenstates as indicated in Figs. 5(a) and (b). As shown in Figs. 5(c) and (d), the maximum of the entanglement amplification is reached when $\phi(t) \simeq -1$. Therefore the dynamic amplification of long-distance entanglement is essen-

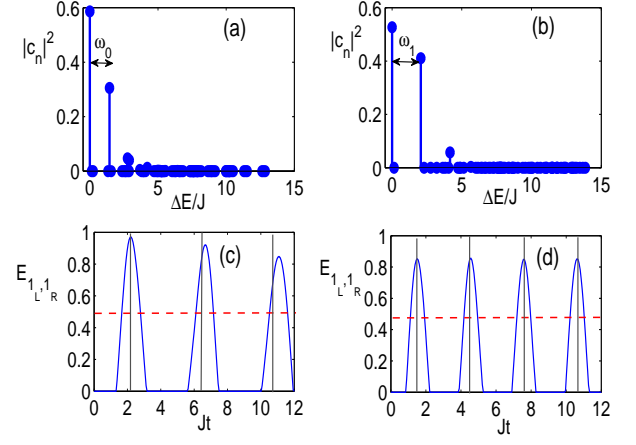


FIG. 5: (Color online) Upper panels: $|c_n|^2$ versus $\Delta E/J = (E_n - E_0)/J$ for all eigenvectors of H_T for two chains with $N_L = N_R = 4$, $J'_L = J'_R = 0.5J$, $J_I = 0.75J$ where J is the bulk amplitude for (a) $\delta = 0$; (b) $\delta = 1$. Lower panels: $E_{1_L, 1_R}$ vs. time for the two chains with parameters given above and (c) $\delta = 0$; (d) $\delta = 1$. The red dashed lines stand for the initial end to end entanglement in each single chain. The vertical gray lines signal the times at which the phase $\phi(t) = \exp(-i\omega_\delta t) = -1$.

tially due to a constructive interference between the two eigenstate while the fact that the maximum is reached around and not exactly at $\phi(t) = -1$ accounts for the projections on the remaining part of the spectrum: although strongly suppressed, they are not exactly vanishing. As we move to values of the Hamiltonian parameters away from the optimal ones and/or the dimension of the two modules is increased, the relative weight of the other eigenstates becomes more relevant reducing the maximum value reached by $E_{1_L, 1_R}$.

It is worth mentioning that in perturbative dynamics we also see the interference between two eigenstates of the Hamiltonian [11–14], however, those eigenvectors have *localized* excitations on edges and have the same structure in the bulk. Due to this minimal difference, i.e. only at the edges where the sender and receiver are located, they are separated by a vanishing energy in the spectrum of the system which results in a very slow dynamics. In contrast, the relevant two eigenstates in our dynamics have completely distinct global structures which also make their energy separations sensibly large and result in our fast dynamics.

VI. IMPERFECTIONS

There are a few imperfection effects which may affect the ideal evolution presented above. Here we consider two main effects: random couplings and thermal fluctuations.

A. Random Couplings

The first effect that we consider here is the randomness in exchange couplings. We assume that $J \rightarrow J(1 + \epsilon)$ where ϵ

λ	0.0000	0.0500	0.1000	0.1500	0.2000
$\langle E_{max} \rangle$	0.7442	0.7256	0.6812	0.6029	0.5391
$\langle E(t_{opt}) \rangle$	0.7442	0.7224	0.6727	0.5839	0.5005
$\langle Jt_{peak} \rangle$	7.2446	7.2427	7.2557	7.2718	7.3007

TABLE I: The effect of random couplings on XX chain of length $N_L = N_R = 8$.

λ	0.0000	0.0500	0.1000	0.1500	0.2000
$\langle E_{max} \rangle$	0.7442	0.6710	0.5941	0.5028	0.4106
$\langle E(t_{opt}) \rangle$	0.7442	0.6380	0.5549	0.4659	0.3820
$\langle Jt_{peak} \rangle$	2.2000	2.1200	2.1000	2.0900	2.0900

TABLE II: The effect of random couplings on a XXX chain of length $N_L = N_R = 8$.

is a dimensionless random number with uniform distribution over $[-\lambda, +\lambda]$. We consider two modules tuned to their optimal values of J_I and J' and a random noise is affecting all the couplings of the system. Due to the random change in the couplings the optimal time at which entanglement peaks may also change. However, determination of this change is only possible if the real values of the random couplings are known. If the real values are not known we have to set the time equal to its value for the clean system. In TABLE I we give the average values of entanglement over 50 different realization of the XX system at its peak (i.e. $\langle E_{max} \rangle$) and the average of entanglement at the optimal time t_{opt} , determined for the clean system (i.e. $\langle E(t_{opt}) \rangle$), for different values of λ . As it is clear from the TABLE I the attainable entanglement deteriorates by increasing λ while the average time at which entanglement peaks changes very slowly. In TABLE 2, the same data for the Heisenberg Hamiltonian is shown. Comparing the two table is possible to see how the XX systems results much more noise resistant than the Heisenberg one. Such fact that is associated to the inner structure of the spectrum of the eigenstate of the Hamiltonian makes the XX model more interesting when in our experimental realization the main source of noise is associated to a lack of precision in the interactions between spins.

B. Thermal Fluctuations

The main issue of exploiting dynamics is to overcome the thermal instability of the static entanglement. In this section we analyze the destructive effect of thermal fluctuations in our system. We assume that the modules cannot be cooled to their ground state and they are initially in a thermal state as $\rho(0) = e^{-(H_L + H_R)/K_B T}$, where T is temperature and K is Boltzmann constant. The evolution of the system is then given by

$$\rho(t) = e^{-iH_T t} \rho(0) e^{+iH_T t}. \quad (6)$$

From $\rho(t)$ one can get the density matrix of the boundary spins by tracing out the rest and compute its entanglement as before.

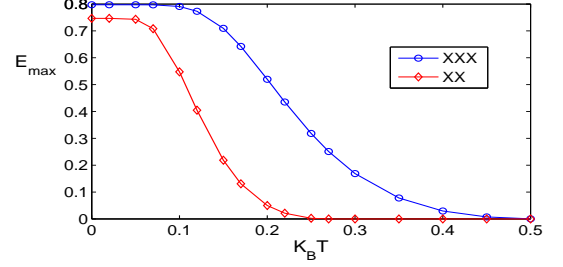


FIG. 6: (Color online) The maximum attainable entanglement versus temperature $K_B T$ in a system of $N_L = N_R = 6$ for the both XX and XXX chains.

In Fig. 6 the E_{max} is plotted as a function of temperature for both XX and XXX chains. As these figures clearly show there is a plateau in small temperatures which its width is proportional to the gap of the system. The wider plateau observed for the Heisenberg chain in compare to the XX one is in fact due to its larger energy gap and results in a better thermal stability for the Heisenberg interaction. Therefore if in our experimental facility we expect that if the greatest source of noise is due to the thermal effects, than we must choose to realize the entanglement amplifier using Heisenberg chains. The time at which entanglement peaks hardly changes with temperature which is in agreement with [22].

VII. CONCLUSIONS & OUTLOOK: ENTANGLEMENT ROUTER

By considering many-body media with static structures of bulk modules and by engineering suitably quenched local interaction dynamics between different modules, we have introduced a method for the generation and amplification of entanglement between distant and non-interacting quantum objects. The method is intrinsically non-perturbative and does not require sophisticated controls of the system dynamics. Indeed, we showed that the end-to-end entanglement initially present in the ground state of a modular many-body system is amplified by the quenched dynamics whenever all the values of the Hamiltonian parameters are far from the perturbative regime. The ensuing entangling dynamics is fast and robust against thermal fluctuations as well as against the presence of noise in the amplitude interactions. The occurrence of such dynamical mechanism of entanglement amplification finds a simple and beautiful explanation in the constructive interference of only two energy eigenstates of the driving Hamiltonian. This opens potentially many new perspective for studying entanglement generation, distribution, and manipulation across arbitrary distances in a many-body systems. Our minimal control strategy applies immediately to the demonstration of an entanglement router capable of distributing entanglement simultaneously between multiple users. Indeed, consider a setup in which every user controls one impurity in a module which extends from its position to a common dispatching center where the other impurities are controlled. In the dispatch-

ing center, one can switch on the interaction between any pair of impurities of different modules and induce the entangling dynamics in those particular chains, thus creating entanglement directly between the two users. The main advantage of such an entanglement router is the minimal control needed (a single bond quench) that, at variance with previous router proposals, neither requires AC-control of the couplings [17] nor the introduction of many different couplings [18]. All this advantages make the present approach suitable of a relatively easy experimental realizations based on different experimental devices as the doped coupling optical cavities [5, 23] or the

trapped ions [24]

Acknowledgements:

AB and MBP acknowledge financial support from the EU STREP project P ICC and the Alexander von Humboldt foundation. SMG and FI acknowledge financial support from the EU STREP Project iQIT, Grant Agreement No. 270843.

-
- [1] M. A. Nielsen and I. L. Chuang, *Quantum Computation and Quantum Information* (Cambridge University Press, Cambridge, 2000).
 - [2] M.B. Plenio, J. Eisert, J. Dreissig and M. Cramer, Phys. Rev. Lett. **94**, 060503 (2005); M.B. Hastings and T. Koma, Comm. Math. Phys. **265**, 781 (2006)
 - [3] L. Campos Venuti, C. Degli Esposti Boschi, and M. Roncaglia, Phys. Rev. Lett. **96**, 247206 (2006).
 - [4] L. Campos Venuti, S. M. Giampaolo, F. Illuminati, and P. Zanardi, Phys. Rev. A **76**, 052328 (2007).
 - [5] S. M. Giampaolo and F. Illuminati, New J. Phys. **12**, 025019 (2010); S. M. Giampaolo and F. Illuminati, Phys. Rev. A **80**, 050301 (2009).
 - [6] G. Gualdi, S. M. Giampaolo, and F. Illuminati, Phys. Rev. Lett. **106**, 050501 (2011).
 - [7] S. Zippili, S. M. Giampaolo and F. Illuminati arXiv:1302.1205.
 - [8] T. Kuwahara, New J. Phys. **14**, 123032 (2012).
 - [9] S. Bose, Contemporary Physics **48**, 13 (2007).
 - [10] J. Eisert, M.B. Plenio, S. Bose and J. Hartley, Phys. Rev. Lett. **93**, 190402 (2004); H. Wichterich and S. Bose, Phys. Rev. A **79**, 060302(R) (2009); K. Sengupta and D. Sen, Phys. Rev. A **80**, 032304 (2009).
 - [11] L. Campos Venuti, C. Degli Esposti Boschi, and M. Roncaglia, Phys. Rev. Lett. **99**, 060401 (2007).
 - [12] M. J. Hartmann, M. E. Reuter, and M. B. Plenio, New J. Phys. **8**, 94 (2006).
 - [13] Y. Li, T. Shi, B. Chen, Z. Song, and C.-P. Sun, Phys. Rev. A **71**, 022301 (2005); A. Wójcik, T. Łuczak, P. Kurzyński, A. Grudka, T. Gdala, and M. Bednarska, Phys. Rev. A **72**, 034303 (2005).
 - [14] M. Bruderer, K. Franke, S. Ragg, W. Belzig, D. Obreschkow Phys. Rev. A **85**, 022312 (2012).
 - [15] A. Bayat, S. Bose, and P. Sodano, Phys. Rev. Lett. **105**, 187204 (2010).
 - [16] L. Banchi, A. Bayat, P. Verrucchi, and S. Bose, Phys. Rev. Lett. **106**, 140501 (2011).
 - [17] D. Zueco, F. Galve, S. Kohler, and P. Hänggi, Phys. Rev. A **80**, 042303 (2009); S. M. Giampaolo, F. Illuminati, A. Di Lisi, and G. Mazzarella, Int. J. Quant. Inf. **4**, 507 (2006); S. M. Giampaolo, F. Illuminati, A. Di Lisi, and S. De Siena, Laser Physics **16**, 1411 (2006).
 - [18] M.B. Plenio, J. Hartley and J. Eisert, New J. Phys. **6**, 36 (2004); P. J. Pemberton-Ross and A. Kay, Phys. Rev. Lett. **106**, 020503 (2011).
 - [19] V. Vedral, M.B. Plenio, M.A. Rippin and P.L. Knight, Phys. Rev. Lett. **78**, 2275 (1997).
 - [20] W.K. Wootters Phys. Rev. Lett. **80**, 2245 (1998).
 - [21] S. Bravyi, D. P. DiVincenzo, and D. Loss, Ann. Phys. (N.Y.) **326**, 2793 (2011).
 - [22] A. Bayat, V. Karimipour, Phys. Rev. A **71**, 042330 (2005).
 - [23] M. J. Hartmann, F. G. S. L. Brandão and M. B. Plenio, Nature Phys. **2**, 849 (2006); A. D. Greentree, C. Tahan, J. H. Cole, and L. C. L. Hollenberg, Nature Phys. **2**, 856 (2006); D. G. Angelakis, M. F. Santos, and S. Bose, Phys. Rev. A **76**, 031805(R) (2007); M. J. Hartmann, F. G. S. L. Brandão and M. B. Plenio, Phys. Rev. Lett. **99**, 160501 (2007).
 - [24] A. Friedenauer, H. Schmitz, J. T. Glueckert, D. Porras, and T. Schaetz, Nature Physics **4**, 757 (2008).